Effect of Ambient Storage on the Degradation of Ni-Rich Positive Electrode Materials (NMC811) for Li-Ion Batteries

Roland Jung,[1,2,3,4,*,z] Robert Morasch,[1,4] Pinar Karayaylali,[4,5] Katherine Phillips,[3,4] Filippo Maglia,[2] Christoph Stinner,[2] Yang Shao-Horn,[3,4,5,6,] and Hubert A. Gasteiger[1,**]**

[1] *Chair of Technical Electrochemistry, Department of Chemistry and Catalysis Research Center, Technische Universität München, Garching, Germany*
[2] *BMW AG, Munich, Germany*
[3] *Research Laboratory of Electronics, Massachusetts Institute of Technology, Cambridge, Massachusetts 02139, USA*
[4] *Electrochemical Energy Laboratory, Massachusetts Institute of Technology, Cambridge, Massachusetts 02139, USA*
[5] *Department of Mechanical Engineering, Massachusetts Institute of Technology, Cambridge, Massachusetts 02139, USA*
[6] *Department of Materials Science & Engineering, Massachusetts Institute of Technology, Cambridge, Massachusetts 02139, USA*

Layered $LiNi_{0.8}Mn_{0.1}Co_{0.1}O_2$ (NMC811) is one of the high-energy positive electrode (cathode) materials for next generation Li-ion batteries. However, compared to the structurally similar $LiNi_{1/3}Mn_{1/3}Co_{1/3}O_2$ (NMC111), it can suffer from a shorter lifetime due to its higher surface reactivity. This work studied and compared the formation of surface contaminations on NMC811 and NMC111 when stored under ambient conditions using electrochemical cycling, Raman spectroscopy, and X-ray photoelectron spectroscopy. NMC811 was found to develop a surface layer of up to ~10 nm thickness that was mostly composed of nickel carbonate species mixed with minor quantities of hydroxide and water after ambient storage for 1 year, while no significant changes were observed on the NMC111 surface. The amount of carbonate species was quantified by gas chromatographic (GC) detection of carbon dioxide generated when the NMC particles were dispersed in hydrochloric acid. Surface impurity species formed on NMC811 upon ambient storage not only lead to a significant delithiation voltage peak in the first charge, but also markedly reduce the cycling stability of NMC811-graphite cells due to significantly growing polarization of the NMC811 electrode.
© The Author(s) 2018. Published by ECS. This is an open access article distributed under the terms of the Creative Commons Attribution Non-Commercial No Derivatives 4.0 License (CC BY-NC-ND, http://creativecommons.org/licenses/by-nc-nd/4.0/), which permits non-commercial reuse, distribution, and reproduction in any medium, provided the original work is not changed in any way and is properly cited. For permission for commercial reuse, please email: oa@electrochem.org. [DOI: 10.1149/2.0401802jes]

BY-NC-ND

Manuscript submitted November 7, 2017; revised manuscript received December 18, 2017. Published January 6, 2018. This was Paper 216 presented at the National Harbor, Maryland Meeting of the Society, October 1–5, 2017.

Secondary Li-ion batteries are alternatives to the combustion engine in vehicles, paving the way to electromobility. Andre et al. have reported that in order to reach a driving range of 300 miles, the specific energy of today's Li-ion batteries needs to be increased to ~750 Wh/kg on a cathode active material (CAM) level, corresponding, e.g., to ~200 mAh/g at an average voltage of ~3.8 V.[1] This demands the development and application of advanced positive electrode (cathode) materials and at the same time requires further improvements with respect to durability and costs for mass market penetration.[1,2] Layered lithium nickel manganese cobalt oxide ($LiNi_xMn_yCo_zO_2$, generally referred to as NMC) is one of the most promising classes of positive electrode materials with $LiNi_{1/3}Mn_{1/3}Co_{1/3}O_2$ (NMC111) being already commercialized for automotive applications.[1,3] However, its reversible capacity only reaches up to ~160 mAh/g_{NMC}[4–7] when cycled at 25°C up to 4.2 V cell voltage in NMC111-graphite full cells (i.e., ~4.3 V vs. Li/Li^+ at discharge rates of 0.1 C) or 4.4 V cell voltage (i.e., ~4.5 V vs. Li/Li^+ at 1 C). The latter results with the observed charge-averaged discharge voltage of ~3.85 V in a specific energy of ~620 Wh/kg,[7] which does not reach the above specific energy target.

Ni-rich NMCs (Ni-content >> Mn- and Co-content) have significantly higher specific capacities. In particular, reversible capacities of ~175–190 mAh/g_{NMC} have been reported for $LiNi_{0.8}Mn_{0.1}Co_{0.1}O_2$ (NMC811) at the lower cutoff voltage of 4.3 V vs. Li/Li^+ and at discharge rates of 0.2-1 C.[5,7,8] However, Ni-rich NMCs frequently exhibit faster capacity fading and shorter lifetime compared to NMC111,[5,9,10] which has in part been attributed to increasing amounts of Ni having more reactive surface oxygen.[11–14] In particular, Gauthier et al. have proposed that the reactivity of the surface oxygen in layered $LiMO_2$ (M = transition metals) can be increased from early to late transition metals, because the oxygen p-band is shifted closer to the Fermi level, rendering greater surface reactivity for NMC811 than NMC111.[11] Whether the proposed higher reactivity of nickel-rich surfaces only reduces their stability when exposed to the ambient or whether for the same state-of-charge (i.e., the same degree of delithiation during charge, controlled by the upper cutoff voltage) nickel-rich surfaces are intrinsically less stable is still unclear.

The high surface reactivity of Ni-rich positive electrodes can lead to the formation of surface impurity species upon reactions with carbon dioxide and water during ambient storage, which can cause problems during electrode slurry preparation, battery storage, and cycling.[15–18] In general, we can distinguish three processes that can be responsible for the presence of surface carbonates and hydroxides, which include i) residual impurities stemming from unreacted precursors during synthesis, ii) a higher equilibrium coverage of surface carbonates/hydroxides required to stabilize the surface of Ni-rich materials after the synthesis process, and/or iii) impurities formed during ambient storage. Paulsen et al. have shown that NMC materials can have different amounts of surface carbonates and hydroxides (referred to as the soluble base content (SBC)), which are dependent on the synthesis conditions such as Li:M ratio, temperature and reaction time.[15] If Li_2CO_3 or LiOH is used as Li-source during the synthesis, stoichiometric conversion is desired (e.g. MOOH + 0.5 Li_2CO_3 → $LiMO_2$ + 0.5 CO_2 + 0.5 H_2O having M = Ni, Co, Mn) as otherwise residual Li_2CO_3 or LiOH precursor would remain on the NMC particle surfaces.[15] When Li_2CO_3 is quantitatively converted, only a low soluble base content is present on the NMC surface.

Even though it appears intuitive to expect that an NMC without any carbonates or hydroxides on the surface should be ideal, Paulsen et al. have reported that the optimal SBC is different from zero, which is referred to as equilibrium SBC. This equilibrium SBC is given as ~20 μmol/g_{NMC} (for NMC622 with a BET surface area of ~0.2 m^2/g) and is proposed to be a surface termination which is required to stabilize the surface of the material and to allow for good cyclability rather than being a detrimental surface impurity.[15] NMCs with an SBC below the desired SBC equilibrium value have poor electrochemical performance.[15] On the other hand, too high carbonate and

*Electrochemical Society Student Member.
**Electrochemical Society Fellow.
[z]E-mail: roland.jung@tum.de

Downloaded on 2020-01-20 to IP 129.187.254.46 address. Redistribution subject to ECS terms of use (see ecsdl.org/site/terms_use) unless CC License in place (see abstract).

hydroxide contents (>150 μmol/g_{NMC}) cause gelation or flocculation during slurry preparation and extensive gassing during high temperature storage of charged battery cells.[15,19]

Upon storage at elevated temperature and/or high humidity, increasing carbonate contents have been reported for the Ni-rich compounds $LiNi_{0.81}Co_{0.16}Al_{0.03}O_2$,[17] $LiNi_{0.8}Co_{0.15}Al_{0.05}O_2$,[18–20] $LiNi_{0.6}Mn_{0.2}Co_{0.2}O_2$,[16] $LiNi_{0.5}Mn_{0.3}Co_{0.2}O_2$,[21] and $LiNiO_2$.[22] At the same time, Shizuka et al. have shown that NMC111 is not sensitive upon storage at 30°C, 80% relative humidity and one month of storage.[18] In most of the previously mentioned studies, the formed carbonate species are assumed to be Li_2CO_3,[12,13,15,17–20,22] although clear evidence for Li_2CO_3 is not presented. Yet, the chemical composition of the surface species is very important to understand the consequences for NMC-graphite cells.

Herein, we compare surface changes on NMC811 with those on NMC111 upon ambient storage, i.e., air storage at room temperature in the absence of excessively high humidity, and report their influence on battery cycling stability. Using X-ray photoelectron spectroscopy (XPS), Raman spectroscopy, and analysis of the carbonate content by gas chromatography (GC) we show that NMC811 is, in contrast to NMC111, sensitive when stored under ambient conditions, forming surface species mainly composed of nickel carbonate mixed with minor amounts of hydroxide and water. The presence of such impurities on NMC811 does not only induce a high initial voltage peak upon delithiation in the first charge, but also causes considerable impedance growth and capacity loss during cycling in NMC811-graphite cells. It is therefore critical to understand the formation and control the amounts of surface impurities on positive electrode materials to allow for low impedance and high cycling stability.

Experimental

Electrode preparation.—NMC electrodes were prepared by dispersing 91.5 $\%_{wt}$ of the active material particles $LiNi_{1/3}Mn_{1/3}Co_{1/3}O_2$ (NMC111, Umicore, Belgium) or $LiNi_{0.8}Mn_{0.1}Co_{0.1}O_2$ (NMC811, Umicore, Belgium), 4.4 $\%_{wt}$ conductive carbon (Super C65, Timcal, Switzerland) and 4.1 $\%_{wt}$ polyvinylidene fluoride binder (PVDF, Kynar HSV 900, Arkema, France) in N-methylpyrrolidone (NMP, anhydrous, 99.5%, Sigma-Aldrich). The powders were weighed in an Ar-filled glovebox (O_2 and H_2O < 0.1 ppm, MBraun, Germany), in which the pristine NMC materials were also stored. The slurry was mixed in a planetary mixer (Thinky, USA) at 2000 rpm for 2 × 5 minutes. In between the two mixing steps, the slurry was ultrasonicated for 10 minutes in an ultrasonic bath to break the agglomerates of the conductive carbon and achieve a more homogeneous mix of active material and Super C65. The resulting ink was spread onto aluminum foil (thickness 18 μm, MTI Corporation, USA) using a gap bar coater (RK PrintCoat Instruments, UK) with a gap size of 250 μm. After drying at 50°C, the electrodes were stored for 3 months (NMC811 3-months) or one year (NMC811 1-year and NMC111 1-year) in the laboratory at ambient air, punched and dried overnight at 120°C under dynamic vacuum in a glass oven (drying oven 585, Büchi, Switzerland) and transferred into a glovebox (O_2 and H_2O < 0.1 ppm, MBraun, Germany) without exposure to ambient air. The storage conditions, i.e., the temperature and humidity in the laboratory were 20–25°C and ~30–50%, respectively. The electrodes labeled as 'fresh' (NMC811 fresh and NMC111 fresh) had no contact to ambient air in any of the process steps, i.e., the slurry was spread onto aluminum, dried, punched and transferred into the glass oven inside the glovebox.

Graphite electrodes were prepared with graphite (MAG-D20, Hitachi), Super C65 (Timcal, Switzerland), sodium carboxymethylcellulose (Na-CMC, Dow Wolff Cellulosics) and styrene-butadiene rubber (SBR, JSR Micro) at a weight ratio of 95.8:1:1:2.2. For the slurry preparation, graphite, Super C65 and Na-CMC were dispersed in highly pure water (18 MΩcm, Merck Millipore, Germany) and mixed in a planetary mixer (Thinky, USA; at 2000 rpm for 30 minutes). Afterwards, the slurry was ultrasonicated for 10 minutes in an ultrasonic bath and SBR was added to the slurry and mixed at 500 rpm for 2 minutes. The ink was coated onto copper foil (thickness 12 μm, MTI Corporation, USA) using a gap bar coater (RK PrintCoat Instruments, UK). After the coating was dried at 50°C in air, electrodes were punched out, dried overnight at 120°C under vacuum in a glass oven (Büchi oven, see above) and transferred into a glovebox without exposure to ambient air.

The specific surface areas of the NMC materials determined by BET are 0.26 m^2/g and 0.18 m^2/g for NMC111 and NMC811, respectively.[7]

Electrochemical characterization.—Voltage profiles of the NMC electrodes were measured in coin cells (Hohsen Corp., Japan) in a half-cell NMC-lithium configuration. Cells were assembled in an argon filled glovebox (O_2 and H_2O < 0.1 ppm, MBraun, Germany) with NMC (14 mm diameter) as working and lithium foil (15 mm diameter, 0.45 mm thickness; battery grade foil, 99.9% purity, Rockwood Lithium, USA) as counter electrode, using two glass fiber separators (glass microfiber filter #691, VWR, Germany), and adding 160 μL LP57 electrolyte (1M $LiPF_6$ in EC:EMC (3:7 wt:wt), <20 ppm H_2O, BASF, Germany). The areal mass loading of the NMC electrodes was 15.3 ± 1 mg_{NMC}/cm^2. The cells were cycled in a climate chamber (Binder, Germany) at 25°C with a battery cycler (Series 4000, Maccor, USA). All cells were cycled 3 times at 0.05 C-rate between 3.0 V and 4.4 V vs. Li/Li^+, with the C-rate being referenced to the approximate reversible capacity of the NMC at 0.05 C, i.e., 170 mAh/g for NMC111 and 210 mAh/g for NMC811. Charging was done in constant current (CC) mode without a constant voltage step.

Electrochemical cycling of NMC811-graphite full-cells was performed in Swagelok T-cells, which were assembled in an argon filled glovebox (O_2 and H_2O < 0.1 ppm, MBraun, Germany), with NMC811 as working electrode (10 mm diameter) and graphite as counter electrode (11 mm diameter). The areal loading of the NMC811 electrodes was 16.4 ± 0.5 mg_{NMC}/cm^2 (2.13 ± 0.07 mAh/cm^2) and the loading of the graphite electrodes was adjusted to yield a constant balancing factor of ~1.2, referenced to the reversible capacities of NMC at a 1 C-rate and a cutoff voltage of 4.1 V vs Li/Li^+ corresponding to 130 mAh/g_{NMC} and of graphite corresponding to 355 mAh/g_C (if referenced to the reversible capacities at 0.1 C, the anode is roughly 1.1-fold oversized in areal capacity). Two glass fiber separators (glass microfiber filter, 691, VWR, Germany) punched to a diameter of 11 mm were used as separators with 80 μL of LP57 (1 M $LiPF_6$ in EC:EMC 3:7 wt/wt, < 20 ppm H_2O, BASF, Germany) electrolyte. The cells were cycled in a climate chamber (Binder, Germany) at 25°C with a battery cycler (Series 4000, Maccor, USA) between cell voltages of 3.0 and 4.0 V. All cells were cycled 300 times at 1 C with two cycles at 0.1 C at the beginning for formation as well as after every 50 cycles. Charging was done in constant current-constant voltage (CCCV) mode with a current limitation corresponding to 0.05 C, while the discharge was done in constant current (CC) mode.

Raman spectroscopy.—All Raman spectra were recorded on a HORIBA Scientific LabRAM HR Raman microscope system (Horiba, Japan) with a He-Ne laser (λ = 632.8 nm) and an objective with a 100-fold magnification to allow the focus on a single NMC particle in the NMC electrodes. Several spots were measured for each sample to assure that the measured spectra are representative for the whole sample. The Raman spectra were measured at air within ~1 h and the samples were not treated prior to the measurement. The following reference compounds (as powders) were used: $NiCO_3$, $MnCO_3$, $CoCO_3$ (Alfa Aesar, USA), $Ni(OH)_2$, Li_2CO_3, $LiOH{\cdot}H_2O$, $(NiCO_3)_2{\cdot}(Ni(OH)_2)_3{\cdot}4H_2O$ (Sigma-Aldrich, USA), and H_2O (18 MΩcm, Merck Millipore, USA). The reference compounds were measured as received without any further purification.

Gas chromatography (GC).—The determination of the carbonate content on the NMC electrodes was accomplished by using the reaction $CO_3^{2-} + 2\,HCl \rightarrow 2\,Cl^- + H_2O + CO_2$ and quantifying the amount of formed CO_2 by means of gas chromatography (GC, SRI 8610C, SRI Instruments, USA). All samples were dried at 120°C under vacuum in a glass oven, weighed in an Ar-filled glovebox (O_2

Downloaded on 2020-01-20 to IP 129.187.254.46 address. Redistribution subject to ECS terms of use (see ecsdl.org/site/terms_use) unless CC License in place (see abstract).

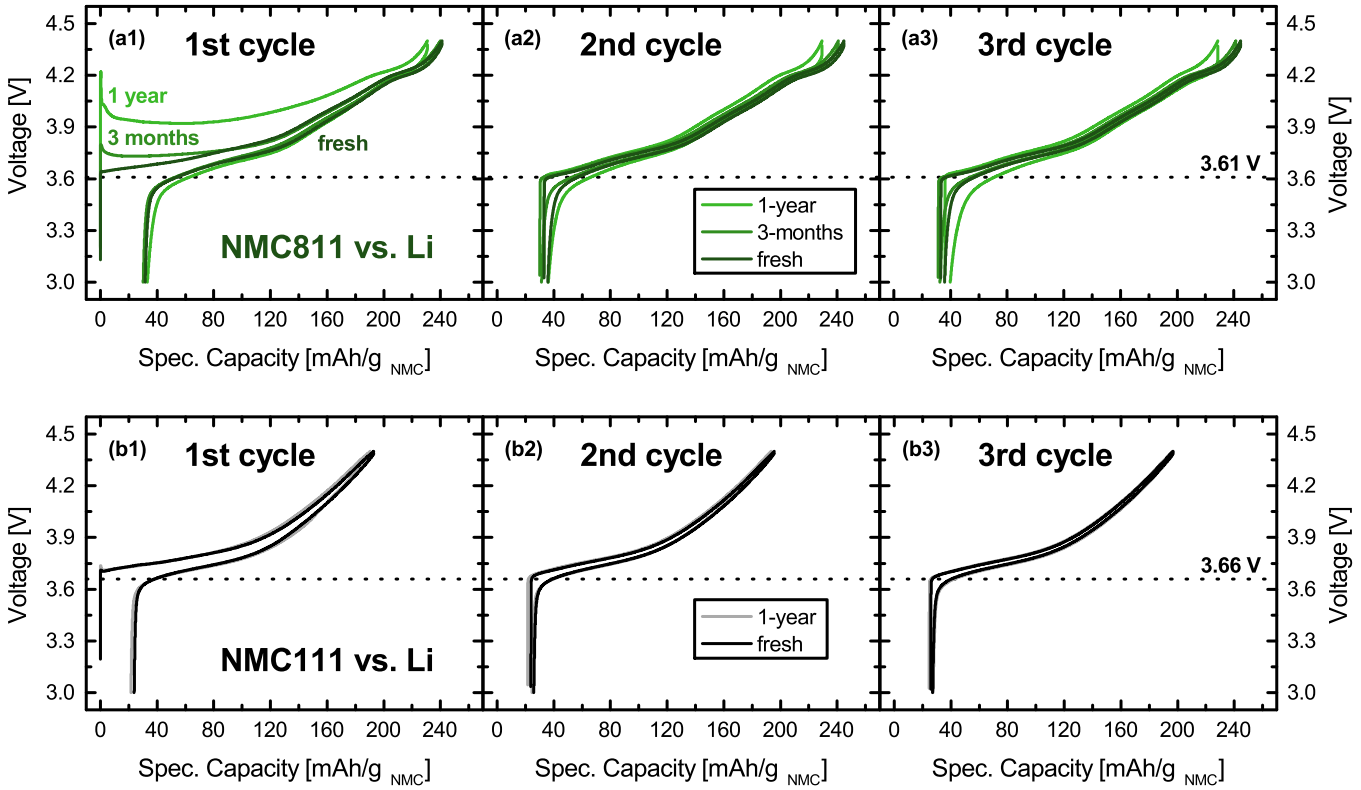

Figure 1. Voltage vs. specific capacity of the 1st, 2nd and 3rd cycle of NMC811-Li (a1, a2 and a3) and NMC111-Li half-cells (b1, b2 and b3) in LP57 electrolyte (1M $LiPF_6$ in EC:EMC 3:7) cycled between cell cutoff voltages of 3.0 V and 4.4 V at a rate of 0.05 C at 25°C (for electrode compositions see Experimental section).

and H_2O < 0.5 ppm, MBraun, USA) and put into 2 mL GC headspace vials (VWR, USA), which were sealed with a cap containing a silicone septum. Outside the glovebox, six droplets of 1.2 M hydrochloric acid were injected with a syringe into the vial. Afterwards, 0.5 mL of the headspace gas volume were drawn into a syringe and injected into the gas chromatograph. In order to quantify the formed amount of CO_2, the gas chromatograph was calibrated using a mixture of Li_2CO_3:NaCl 1:999 (wt:wt) prepared and measured in the same way as the samples.

X-ray photoelectron spectroscopy (XPS).—XPS spectra were measured using a PHI 5000 VersaProbe II (ULVAC-PHI, Japan) X-ray photoelectron spectrometer. The NMC electrodes were mounted in an Ar-filled glovebox (O_2 and H_2O < 0.5 ppm, MBraun, USA) onto the sample holder, put into a transfer vessel and dried for three hours in the small glovebox antechamber under dynamic vacuum. The transfer vessel was sealed to avoid contact to ambient air and transferred into the introduction chamber of the XPS spectrometer. The introduction chamber was evacuated and the samples were transferred to the XPS analysis chamber and measured at room temperature using a monochromatic Al-K_α (1486.6 eV) X-ray source and a spot diameter of 200 µm. All spectra were calibrated with the carbon 1s photoemission peak for adventitious hydrocarbons at 285.0 eV and background corrected using a Shirley background.

Results

Voltage profiles of fresh and aged NMC811 and NMC111.—Figure 1 shows the voltage profiles of the first three cycles of NMC811-Li (panels a1, a2 and a3) and NMC111-Li half-cells (panels b1, b2 and b3). The electrodes were stored at ambient air for one year (NMC811 1-year and NMC111 1-year), three months (NMC811 3-months), or had no contact to ambient air (NMC811 fresh and NMC111 fresh). Note, that after storage the electrodes were dried at 120°C under dynamic vacuum to remove moisture prior to cell assembly (see Experimental section). In the first cycle of the NMC811 samples (Figure 1a), an initial voltage peak appears at the very beginning of the charging process, similar to the observations in the literature for $LiNiO_2$,[22] NMC532,[21] and NMC622.[16] Its magnitude, i.e., the maximum initial peak voltage increases the longer the electrode was exposed to ambient air and reaches 3.80 V and 4.22 V for the 3-months old and for the 1-year old samples, respectively. In comparison, for the fresh sample no initial voltage peak is observed and delithiation of the NMC811 not exposed to the ambient starts at ~3.64 V. After the fresh and 3-months old samples are charged to ~80 mAh/g_{NMC}, their voltage profiles merge and no significant differences between the two coatings can be detected anymore. In contrast, the profile of the 1-year old sample does not merge with that of the fresh sample and reaches the cutoff voltage of 4.4 V at a specific capacity of 231 mAh/g_{NMC}, which is significantly lower than the specific capacity of 241 mAh/g_{NMC} reached by both the fresh and 3-months old samples. Furthermore, the charging curve of the 1-year old sample lies at higher voltages, indicating a larger resistance.

In the second and third cycle, the voltage profiles of the fresh and 3-months old samples are essentially identical, while the capacity of the 1-year old sample is lower and its charging potential remains at higher voltages, again indicating a larger resistance, albeit less severe as during the first charge (Figure 1a2 and a3). Additionally, the initial voltage peak feature of the aged samples is not anymore observed in the second and third cycles, and delithiation starts for all samples at ~3.61 V. This value is significantly lower than the 3.68 V, 3.73 V and 3.93 V, which were measured in the first cycle for the same degrees of delithiation of the fresh, 3-months and 1-year old samples, respectively (note that due to the irreversible capacity in the first cycle the here compared voltages are the values measured at ~31 mAh/g_{NMC}). This difference between the first and subsequent cycles indicates that

Downloaded on 2020-01-20 to IP 129.187.254.46 address. Redistribution subject to ECS terms of use (see ecsdl.org/site/terms_use) unless CC License in place (see abstract).

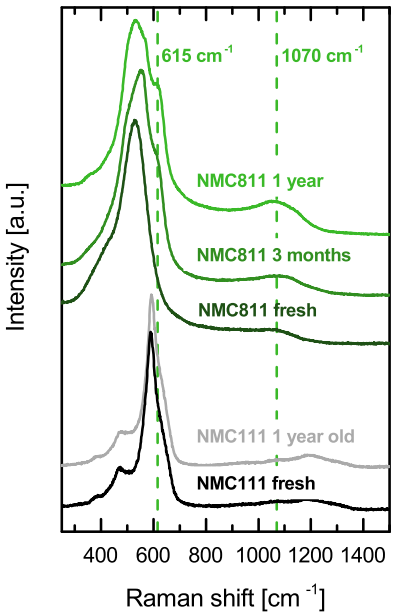

Figure 2. Raman spectra of the NMC111 and NMC811 electrodes shown in Figure 1 before cycling. The Raman spectra were measured at air within ~1 h and the samples were not treated prior to the measurement. The vertical dashed lines mark the bands of the impurities formed on NMC811 during storage at ambient air.

the reason causing the initial voltage peak for the stored samples might also be occurring on the fresh sample, albeit to a much lesser degree.

As the initial voltage peaks occurred when the electrodes were stored under ambient conditions, the formation of surface impurities is the most likely explanation. The most common impurities which can be formed by storage at ambient air are hydroxides via the reaction of the NMC surface with humidity as well as carbonates via the reaction of CO_2 with the initially formed surface hydroxides. It is known that the formation of surface impurities is more significant on Ni-rich NMC materials,[16–19,21,22] which would be consistent with the observed unchanged voltage profile and capacity after one year of ambient storage for NMC111 (see text below) in contrast to NMC811. The formation of hydroxide/carbonate surface impurities on Ni-rich surfaces could also explain the observed initial voltage peak feature, as these would likely form an insulating and therefore resistive layer covering the active material particles. Consequently, the absence of the initial voltage peak in subsequent cycles indicates that the impurity might be (at least partially) decomposed during the first charge.

In Figure 1b, similar experiments are shown for NMC111 both without ambient air exposure (NMC111 fresh) or stored for one year at ambient air (NMC111 1-year). In the first cycle (Figure 1b1) after one year of storage, only a very small initial voltage peak at the beginning of charge is observed, which has its maximum at 3.74 V. In comparison, for the fresh sample no peak is visible and delithiation starts around 3.71 V. Besides this rather small feature, the voltage profiles of the two NMC111 samples are essentially indistinguishable and their specific capacity at 4.4 V in the first cycle is 193 mAh/g_{NMC}. As in the case of the NMC811 samples, in the subsequent cycles no peak feature is observed for any of the samples and delithiation starts at ~3.66 V. At a comparable delithiation state in the first cycle, the measured voltage is 3.73 V (values measured at ~22 mAh/g_{NMC}). In analogy to the experiments with NMC811 (Figure 1a), this difference indicates the presence of a surface film also on the fresh sample, however, no significant changes occur during storage at ambient air. The presence of carbonates on fresh NMC111 would be consistent with the literature[5,15] and might be the reason for the slight difference between the first and the second cycle. A more detailed discussion on the difference of the initially present carbonate coverage to the one formed during storage for NMC811 will follow in the Discussion section.

Identification of the surface impurities upon ambient storage.— In order to examine the hypothesis that increasing amounts of carbonate and/or hydroxide species on the NMC surface lead to the initial voltage peak feature in the first charge (see Figure 1), we analyzed the electrodes using Raman spectroscopy. The measured Raman spectra of the electrodes examined in Figure 1 before cycling are displayed in Figure 2. For NMC111, two bands can be distinguished at 474 cm^{-1} and 591 cm^{-1}. As reported by Kerlau et al., these two bands are actually composed of bands at 474 cm^{-1} and 554 cm^{-1} corresponding to the Ni-O vibrations, at 594 cm^{-1} (Mn-O vibrations), and at 486 cm^{-1} and 596 cm^{-1} (Co-O vibrations), which are partially merged into one broad band.[23] For fresh NMC811, only one clear band is observed with a maximum intensity at 528 cm^{-1}; its shift to lower wave numbers compared to NMC111 can be explained by considering that for NMC811 the fraction of the Ni-O vibrations, which are observed at the lowest wave numbers, increase at the expense of the Mn-O and Co-O vibrations. As one might expect based on the cycling data presented in Figure 1, no significant differences of the Raman spectra are observed for fresh and 1-year old NMC111 (black and gray spectra in Figure 2). In contrast, the spectra of the NMC811 samples change considerably over the storage time. In particular, a shoulder in the NMC peak evolves with its maximum at ~615 cm^{-1}, and the initially rather small peak at ~1070 cm^{-1} in the fresh sample grows significantly after three months and even more after a year. We also measured Raman spectra of NMC811 electrodes dried at 120°C under dynamic vacuum, yet we observed no difference for any of the electrodes, i.e., the additional bands at ~615 cm^{-1} and ~1070 cm^{-1} are not removed during drying, which is in agreement with a very recent report by Faenza et al.[20]

To investigate the origins of the evolving Raman signals at ~615 cm^{-1} and ~1070 cm^{-1}, we compared the spectra of the battery materials with those of several carbonate and hydroxide compounds. Figure 3 depicts the Raman spectra of Li_2CO_3, $NiCO_3$, $CoCO_3$, $MnCO_3$, $LiOH^*H_2O$, $Ni(OH)_2$, H_2O, $NiCO_3{}^*x\,H_2O$, $Ni(OH)_2{}^*x\,H_2O$, and $(NiCO_3)_2{}^*(Ni(OH)_2)_3{}^*4\,H_2O$ in comparison to the 1-year old NMC811 sample. Around 1070 cm^{-1}, NMC811 has a broad band (see uppermost spectrum), and it can be seen that the carbonates Li_2CO_3, $NiCO_3$, $CoCO_3$, and $MnCO_3$ (lowermost spectra) have a band that fits very well to the one observed for the NMC811 sample. In contrast to Li_2CO_3, $NiCO_3$, and $CoCO_3$, additional bands were measured for $MnCO_3$ which originate from H_2O (see the Raman spectra of H_2O in Figure 3 for comparison) due to residual moisture in the sample. A band around 1070 cm^{-1} is also observed for $LiOH * H_2O$, however, we believe that it is due to some Li_2CO_3 impurity in the $LiOH * H_2O$ (formed by a reaction of LiOH with CO_2 in air), which unfortunately is a common impurity.[24] Therefore, the band around 1070 cm^{-1} indicates that carbonates are formed on the surface; however, it is inconclusive which carbonate(s) might be present (i.e., Li_2CO_3 and/or transition metal carbonates). The fact that these surface impurities are only observed in the Raman spectra of aged NMC811 and not for aged NMC111 strongly suggests that the formation of the surface contamination is related to the nickel-content. More precisely, it may be related to the Ni^{3+} content, which is larger in the Ni-rich NMCs compared to layered oxides with low Ni-content.

In the region around the band at 615 cm^{-1} (Figure 3), it is clearly visible that this peak does not match with any of the carbonates nor with $LiOH * H_2O$. Also, $Ni(OH)_2$ does not have a band in this region; instead, water has a band close to 600 cm^{-1} (Figure 3), which might be the origin of the band at 615 cm^{-1} if it shifts when it is bound as crystal water rather than free water. To test this hypothesis, water was added to both $NiCO_3$ and $Ni(OH)_2$ and dried at 60°C under dynamic vacuum to remove most of the free water. For $NiCO_3$ mixed with water (labelled $NiCO_3{}^*xH_2O$ in Figure 3), only the sum of the water and $NiCO_3$ spectra is measured, with no shifts of any band. In contrast, for $Ni(OH)_2$ the Raman spectrum slightly changes, indicating the formation of a hydrate. In particular, $Ni(OH)_2{}^*xH_2O$ has the maximum intensity of

Downloaded on 2020-01-20 to IP 129.187.254.46 address. Redistribution subject to ECS terms of use (see ecsdl.org/site/terms_use) unless CC License in place (see abstract).

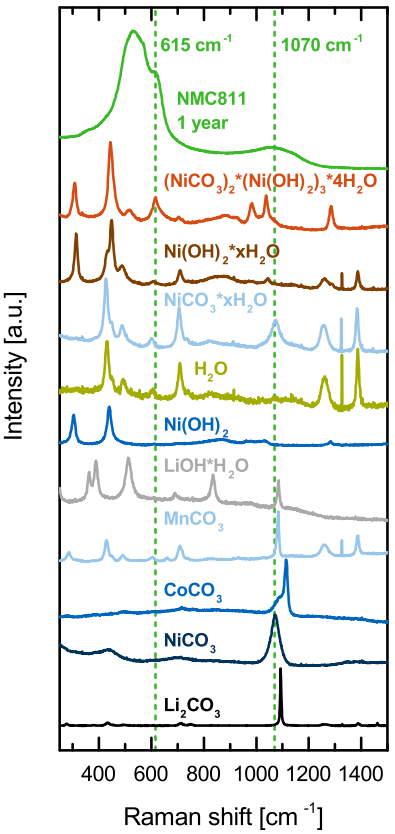

Figure 3. Raman spectra of the 1 year old NMC811 electrodes (same as in Figure 2) and of several carbonate and hydroxide reference compounds (as powders).The reference compounds were measured as received without any further purification.

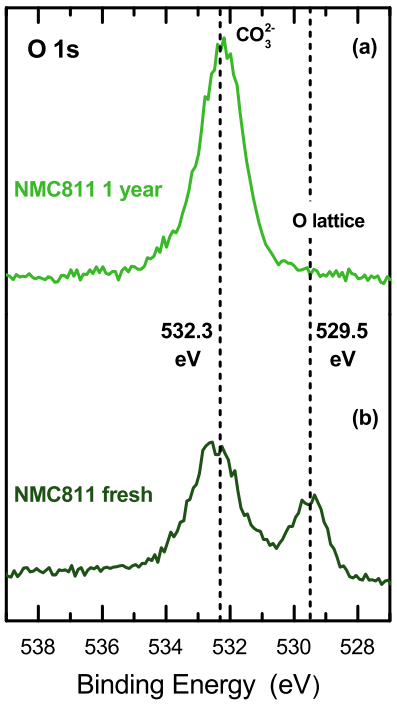

Figure 4. XPS spectra of the Oxygen 1s photoemission lines for the 1 year old (a) and fresh (b) NMC811 electrodes.

the largest band at 448 cm^{-1} and a shoulder at 433 cm^{-1}. Water-free $Ni(OH)_2$ has a band at 439 cm^{-1} and water has its largest band at 430 cm^{-1} with a shoulder at 449 cm^{-1}. The band at 488 cm^{-1} of water slightly shifts to 493 cm^{-1} in $Ni(OH)_2{*}xH_2O$. However, no significant shift was observed for the band around 600 cm^{-1} and its relative intensity even decreased. Lastly, the hydrate of the mixed crystal of nickel carbonate and hydroxide (labelled $(NiCO_3)_2{*}(Ni(OH)_2)_3{*}4H_2O$) was measured. For this compound, the band at 615 cm^{-1} is clearly visible, which shows that mixed crystals of hydroxides and carbonates display significantly altered Raman spectra compared to the pure compounds. This observation makes it very likely that a mixed hydrous carbonate hydroxide is formed, rather than two separate compounds. By comparing the Raman spectrum of this compound with the 1-year old NMC811 sample, it can be seen that the peaks at 307 cm^{-1}, 444 cm^{-1}, and 1286 cm^{-1} are not visible in the NMC811 sample. As these peaks clearly originate from the pure hydroxide or water, the mixed carbonate hydroxide compound formed on the NMC811 surface should have a much larger fraction of carbonate compared to hydroxide and water ($(NiCO_3)_x \cdot (Ni(OH)_2)_y \cdot zH_2O$ with $x \gg y, z$). This can be rationalized by considering that the hydroxide and crystal water can react with CO_2 to form the carbonate, thereby shifting the overall composition in favor of the carbonate. Also, as we did not store the material under excessively high humidity, we believe that this favors the formation of carbonates. Additionally, the bands around 1000 cm^{-1} for $(NiCO_3)_2{*}(Ni(OH)_2)_3{*}4H_2O$, which are significantly shifted compared to the pure carbonate, might cause the broadness of the band observed for the NMC811 around 1070 cm^{-1}, which is fairly narrow for the pure carbonates. While the involvement of Li and the other transition metals (Mn and Co) in the carbonate hydroxide hydrates cannot be excluded, the fact that the surface impurity is only formed on NMC811 and not on NMC111 indicates that Ni is essential for the formation of the surface film. Additionally, to the best of our knowledge, mixed crystals of Li_2CO_3 and LiOH do not exist and the shoulder at 615 cm^{-1} cannot be explained by the pure lithium compounds. Therefore, an involvement of nickel in the surface impurity appears very likely and the commonly stated assumption that all the impurities are due to LiOH and Li_2CO_3[12,13,15,17–19,22] would be inconsistent with our data and thus seems incorrect.

To gain further insight into the chemical nature of the surface impurity, XPS spectra were measured. Figure 4 depicts the oxygen 1s spectra of the 1-year old (a) and fresh (b) NMC811 samples. For the fresh sample, two well-separated peaks are observed at 532.3 eV, which corresponds to carbonate,[25,26] and at 529.5 eV[26] corresponding to the NMC lattice oxygen. The presence of carbonate even on the fresh sample is in agreement with the literature,[5,15] the Raman spectra (Figure 3), and the voltage profiles (Figure 1). In the 1-year old sample, the peak corresponding to the lattice oxygen is not visible anymore and only the intense carbonate peak can be observed, consistent with the observations by Shkrob et al.[21] and Liu et al.[22] This clearly indicates the growth of a surface layer of carbonate species covering the lattice oxygen on the surface of the 1-year old sample. As described by Seah et al., the inelastic mean free path of an electron can be estimated by $\lambda = B \cdot E^{0.5}$ with E being the energy of the photoelectron (in units of eV) and B being a material constant, which they showed to be around 0.096 nm for inorganic compounds.[27] For the ~1000 eV of the O 1s photoelectron (~1500 eV of the incident beam minus ~500 eV binding energy), the calculated inelastic mean free path is ~3 nm. Using Lambert-Beer's law, the O 1s lattice oxygen signal would decay to ~3% (and thus become undetectable in our measurements), if the surface were covered with an impurity layer of ~10 nm. Hence, the absent lattice oxygen signal for the 1-year old sample indicates that the surface contamination after one year of storage at ambient air should have a thickness in the range of ~10 nm, as discussed in more detail in the Discussion section. Additionally, the absence of a clearly pronounced hydroxide peak at 530.8 – 531.1 eV for LiOH[26,28,29] or at 530.8 – 531.0 eV for $Ni(OH)_2$[30,31] indicates only minor fractions of hydroxides on both the fresh and 1 year old sample, consistent with the expectations based on the Raman spectra (Figure 3) and previous reports in the literature.[17–19,22]

Downloaded on 2020-01-20 to IP 129.187.254.46 address. Redistribution subject to ECS terms of use (see ecsdl.org/site/terms_use) unless CC License in place (see abstract).

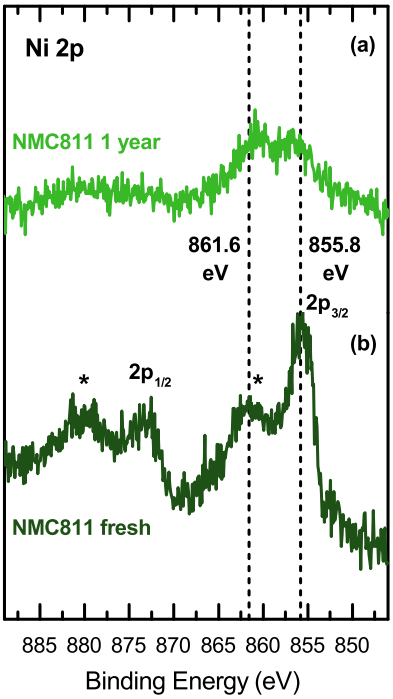

Figure 5. XPS spectra of the Nickel 2p photoemission lines for the 1 year old (a) and fresh (b) NMC811 electrodes. The peaks marked by a * are the satellites of the respective $2p_{3/2}$ and $2p_{1/2}$ peaks.

Figure 5 shows the corresponding nickel 2p spectra of the above discussed samples. The fresh NMC811 sample has two peaks, which are due to the spin-orbit splitting of the Ni 2p states ($2p_{3/2}$ and $2p_{1/2}$), and one satellite (marked by *) for each of the two 2p-states in analogy to $LiNi_{0.5}Co_{0.5}O_2$[32] and $LiNiO_2$.[22] For the NMC811 sample after storage in air for one year, the $2p_{3/2}$ peak slightly shifts to higher binding energies, while its satellite shifts to lower binding energies. Interestingly, this is in contrast to the report by Liu et al.[22] who observed a significant shift by 1.5 eV toward lower binding energies for the Ni $2p_{3/2}$ peak of $LiNiO_2$ after one year of ambient storage. However, they also detected a fraction of ~13% of Li_2CO_3 of the total electrode material weight which is roughly 30-times more than what we detected (see below). Additionally, in Figure 5 the satellite peaks become larger with respect to the non-satellite peaks. While this feature is hard to interpret, the even more interesting observation is that nickel species are still visible after one year even though the lattice oxygen signals measured at the same time on the same sample is not visible anymore (see Figure 4). This is important, because the sensitivity for nickel is even lower than for oxygen (based on the above equation, the inelastic mean free path for Ni 2p is only ~2.5 nm compared to ~3 nm for O 1s), and if nickel would only be present in the NMC lattice and not in the surface impurity layer, it should not be detectable on the 1-year stored NMC811 as is the case for lattice oxygen. This observation demonstrates that nickel is still on the surface, but now bound in the surface impurity layer.

We also measured carbon 1s spectra, however, since the electrodes contain both Super C65 carbon as well as PVDF no conclusions can be drawn from these spectra.

Quantification of the surface impurities upon ambient storage.— Raman spectroscopy and XPS indicate that the vast majority of the formed contamination is carbonate, so that a quantification of the carbonate content is expected to be close to the total impurity content. For quantification, we applied gas chromatography as it has very low detection limits, good sensitivity, and allows the use of very low sample amounts of the electrode coatings. For the determination of the carbonate content we made use of the reaction $CO_3^{2-} + 2\ HCl \rightarrow 2\ Cl^- + H_2O + CO_2$ and quantified the amount of formed CO_2 (see Experimental section). The results are summarized in Table I and show that the fresh NMC111 and NMC811 electrode samples have very similar initial carbonate contents of 0.07 – 0.08$\%_{wt}$ The presence of carbonate on the fresh sample is consistent with the results obtained by XPS (Figure 4).

Table I. Mass fractions of CO_3^{2-} in $\%_{wt}$ on the NMC surface measured by gas chromatographic analysis of fresh and aged electrodes (error bars represent the standard deviation from at least four repeat measurements) as well as the calculated carbonate layer thickness assuming a compact layer with the crystallographic density $\rho = 4.358\ g/cm^3$ [33] of $NiCO_3$.

	CO_3^{2-} mass fraction [$\%_{wt}$]	Layer thickness [nm]
NMC811 fresh	0.08 ± 0.01	2.0 ± 0.3
NMC811 3-months	0.27 ± 0.05	6.8 ± 1.2
NMC811 1-year	0.39 ± 0.06	9.8 ± 1.5
NMC111 fresh	0.07 ± 0.02	1.2 ± 0.4
NMC111 1-year	0.08 ± 0.01	1.4 ± 0.2

If the mass ratios of carbonate were to be converted to lithium carbonate to compare it to the literature, the given values in Table I have to be multiplied by the ratio of the molar masses M of lithium carbonate and carbonate, i.e., $M(Li_2CO_3)/M(CO_3^{2-}) = 1.23$. For the fresh NMC111 and NMC811 electrodes, this would yield 0.09 and 0.1 $\%_{wt}$ Li_2CO_3, respectively, which is very close to the commonly reported values for NMC111.[5] During storage at ambient air, the carbonate content on NMC111 remains essentially constant, consistent with the voltage profiles (Figure 1b) and Raman spectra (Figure 2) which are identical for fresh and aged NMC111 electrodes. In contrast, the carbonate contents of NMC811 electrodes increase significantly from 0.08$\%_{wt}$ (fresh) to 0.27$\%_{wt}$ after three months and to 0.39$\%_{wt}$ after one year of ambient storage, which matches the expectations based on the voltage profiles (Figure 1a) and Raman spectra (Figure 2 and Figure 3). The theoretical layer thickness of the formed surface film during storage is shown in the last column of Table I. Thus the estimated layer thickness of ~10 nm for the 1-year aged NMC811 electrode is consistent with the fact that no lattice oxygen O 1s signal can be observed anymore for this sample (see Figure 4); this will be discussed further in the Discussion section.

Cycling of NMC811-graphite full-cells.—To investigate the impact of the surface contamination on full-cells, NMC811-graphite T-cells equipped with a lithium reference electrode were cycled over 300 times and their discharge curves were compared. Figure 6a shows the specific discharge capacity (left y-axis) and coulombic efficiency (right y-axis) of these cells vs. cycle number. Note that in contrast to the voltage profiles depicted in Figure 1, the upper cutoff voltage was limited to 4.0 V cell potential (~4.1 V vs. Li/Li^+ for the NMC cathode), which we showed in a recent publication to be the limit for the here used NMC811 material in order to avoid significantly growing cathode impedances due to the release of lattice oxygen from the surface of the NMC811 particles[7] (note that the upper cutoff potential limit for stable cycling performance might be different for NMC811 from different suppliers). As expected based on the voltage profiles and capacities shown in Figure 1, the initial capacities both at 1 C (solid lines) and 0.1 C (single data points) of the fresh and 3-months old electrodes are similar, but very different to the 1-year old sample. This underlines the significant damage to the material after one year of storage at ambient air. Interestingly, the specific capacity of the 1-year old NMC increases significantly over the first ~25 cycles, analogous to what was reported for NMC532[21] over the course of a short 4-cycle test. We believe this is due to a more incomplete decomposition of the carbonate species within the first cycles, as the upper cutoff voltage was reduced compared to the data in Figure 1 (note that the initial voltage peak on the 1-year aged NMC811 electrode was at 4.22 V vs. Li/Li^+, which is slightly above the upper cutoff voltage used for Figure 6). Table II summarizes the specific capacity and energy retentions

Downloaded on 2020-01-20 to IP 129.187.254.46 address. Redistribution subject to ECS terms of use (see ecsdl.org/site/terms_use) unless CC License in place (see abstract).

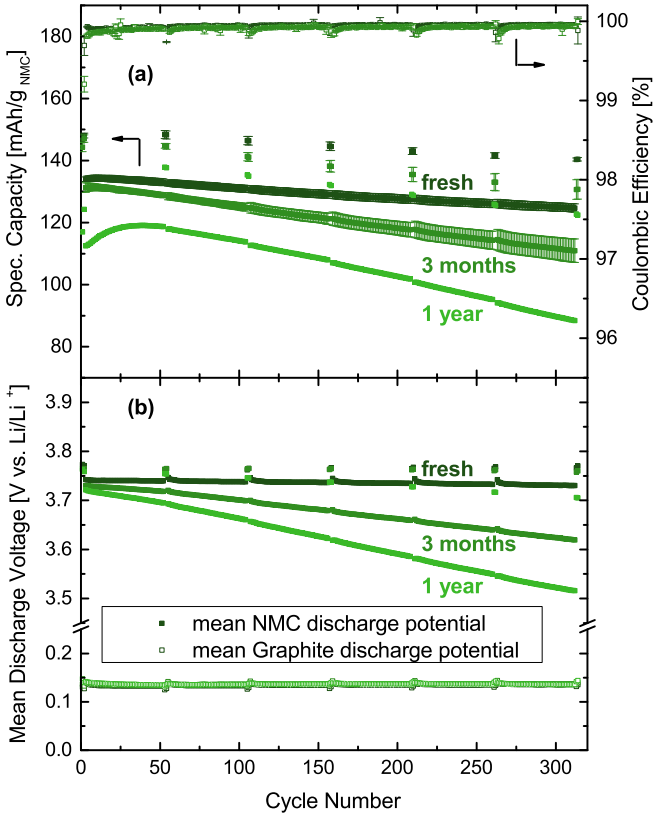

Figure 6. (a) Specific discharge capacity and coulombic efficiency of NMC811-graphite full-cells equipped with a lithium reference electrode for NMC811 cathodes which had no contact to ambient air (fresh) or which were stored for either 3 months or 1 year at ambient air prior to cell assembly. (b) Charge-averaged mean discharge voltage (s. Eq. 1) of the NMC811 cathodes ($\equiv \bar{V}^{cathode}_{discharge}$; full squares) and the graphite anodes ($\equiv \bar{V}^{anode}_{discharge}$; blank squares) vs. cycle number in LP57 electrolyte (1 M $LiPF_6$ in EC:EMC 3:7). The cells were operated between 3.0 V and 4.0 V cell potential at 25°C. Formation was done at a rate of 0.1 C (2 cycles) and cycling was performed at 1 C with two cycles at 0.1 C after every 50 cycles. The error bars for the fresh and 3-months electrodes represent the standard deviations of two repeat measurements.

of the cells depicted in Figure 6. The cells with fresh NMC811 have a very stable cycling performance (dark green squares), with a specific discharge capacity of 134 mAh/g_{NMC} in cycle 4 and 125 mAh/g_{NMC} in cycle 312 (both at a 1 C-rate) corresponding to a capacity retention of 93%. In contrast, the cells containing the 3-months old NMC811 (green squares) fade from 131 mAh/g_{NMC} (cycle 4) to 111 mAh/g_{NMC} (cycle 312), yielding a lower capacity retention of 84%. Lastly, the 1-year old NMC811 exhibits the poorest performance with a capacity of only 88 mAh/g_{NMC} in cycle 312 (light green line). Due to the increasing capacity for the first ~50 cycles we chose the capacity of 118 mAh/g_{NMC} measured in cycle 55 as 'initial' capacity yielding a capacity retention of 75%. The capacity retentions at a 0.1 C-rate are 94% and 89% for the fresh and the 3-months aged NMC811 (cycle 2 to 314) and 88% for the 1-year old NMC811 (cycle 54 to 314). The almost equal capacity retentions for the fresh samples at both C-rates indicate the absence of a significant impedance growth. This is in contrast to the 3-months and 1-year old samples which have higher capacity fading rates at 1 C compared to 0.1 C, as is summarized in Table II. The averaged coulombic efficiencies for the fresh and 3-months old samples at 1 C are >99.9%. For the 1-year old sample the coulombic efficiency in the first 50 cycles is in average ~99.8% and increases to >99.9% in the subsequent cycles.

In order to better understand how the formation of surface impurities causes poorer cycling performance, the charge-averaged mean discharge voltage of the NMC and the graphite electrodes are plotted in Figure 6b. The charge-averaged mean discharge voltage is defined according to Eq. 1 and can be used to monitor changes in the polarization during cell discharge.

$$\bar{V}_{discharge} = \int V_{discharge} \cdot dq_{discharge} \,/\, \int dq_{discharge} \qquad [1]$$

As the cells were cycled with a lithium reference electrode, $\bar{V}_{discharge}$ can be determined independently for the NMC811 cathode ($\equiv \bar{V}^{cathode}_{discharge}$) and the graphite anode ($\equiv \bar{V}^{anode}_{discharge}$) as a function of the cycle number, which is depicted by the full and blank squares in Figure 6b, respectively. It can be seen that $\bar{V}^{anode}_{discharge}$ is perfectly constant for all NMC811 electrodes over the 314 cycles (the small deviations every 50th cycle are caused by the change between C-rates of 1 C and 0.1 C). This independence of $\bar{V}^{anode}_{discharge}$ for fresh and aged NMC811 cathodes indicates that there is no significant cross-talk between anode and cathode,[34–36] i.e., while the impurity level of the various NMC811 electrodes obviously affects capacity retention (Figure 6a), it does not seem to affect the graphite anode (e.g., by releasing any soluble species into the electrolyte, which could be deposited on the graphite and thus would be expected to affect its impedance). In contrast, $\bar{V}^{cathode}_{discharge}$ strongly depends on the extent of aging of the NMC electrodes. In particular, in cycle 3 (i.e., the 1st cycle at 1 C), $\bar{V}^{cathode}_{discharge}$ is highest for the fresh and lowest for the 1-year old NMC811 electrodes, indicating a larger initial impedance on the stored NMC samples. During cycling, the mean discharge voltage of the fresh NMC811 cathodes remains essentially constant; however, a significant decrease in the mean discharge voltage is detected for the 3-months and even more so for the 1-year old NMC811 cathodes. Therefore, it is clear that the buildup of surface impurities during exposure to the ambient causes a higher initial impedance, which gradually increases during cycling concomitant with a deterioration of the NMC811-graphite cell performance. The impedance buildup is further supported by the fact that the difference between the mean discharge voltages of the 1-year old and the fresh NMC811 electrodes at 0.1 C only grows from ~10 mV (2nd cycle) to ~65 mV (314th cycle), in contrast to the much larger difference developing at 1C, starting at ~20 mV (3rd cycle) and ending at ~210 mV (312th cycle). Quite clearly, surface impurities produced during exposure of NMC811 to the ambient do not only deterioriate

Table II. Measured specific capacity and specific energy retentions in NMC-graphite full-cells between the 4th and 312th cycle at 1C and between the 2nd and 314th cycle at 0.1 C of the fresh and 3-months old NMC811 electrodes and between the 55th and 312th (1C) and the 54th and 314th cycle (0.1 C) of the 1-year old NMC811 electrodes extracted from the data depicted in Figure 6. The values in brackets are the specific capacities (left columns) in units of mAh/g_{NMC} and the specific energies (right columns) in units of mWh/g_{NMC} of the respective cycles.

	specific capacity		specific energy	
	1 C	0.1 C	1 C	0.1 C
NMC811 fresh	93 % (134 → 125)	94 % (149 → 140)	93 % (483 → 448)	94 % (541 → 510)
NMC811 3 months	84 % (131 → 111)	89 % (147 → 131)	82 % (472 → 386)	87 % (534 → 474)
NMC811 1 year	75 % (118 → 88)	88 % (138 → 122)	71 % (419 → 299)	87 % (501 → 435)

Downloaded on 2020-01-20 to IP 129.187.254.46 address. Redistribution subject to ECS terms of use (see ecsdl.org/site/terms_use) unless CC License in place (see abstract).

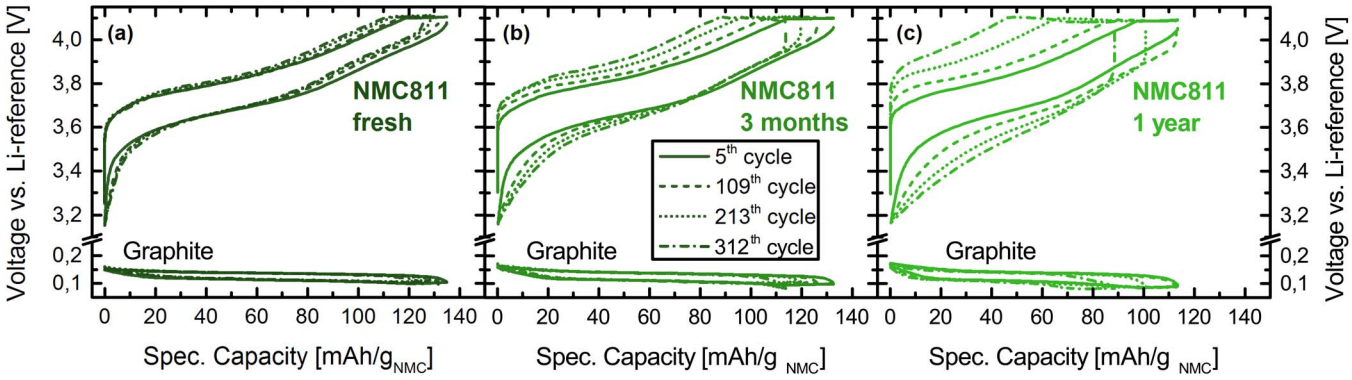

Figure 7. Voltage profiles of the 5th, 109th, 213th, and 312th cycles (all at 1 C-rate) of the cells depicted in Figure 6. The voltage profiles of the NMC811 cathode and graphite anode are shown versus the Li-reference electrode. The NMC811 cathodes had (a) no contact to ambient air or were stored for (b) 3 months or (c) 1 year at ambient air.

its initial capacity and mean discharge voltage, but also lead to an increasing impedance growth over extended charge/discharge cycles.

From Figures 6a and 6b the discharge energy for each cycle can be calculated as the product of capacity and $\bar{V}_{discharge} = \bar{V}^{cathode}_{discharge} - \bar{V}^{anode}_{discharge}$. Due to the substantially decreasing mean discharge voltage of the 3-months and 1-year old samples at 1 C-rate, their specific energy retentions (right-hand columns in Table II) are lower than the capacity retentions, contrary to the nearly identical capacity and energy retention of the fresh sample. At the lower rate of 0.1 C, the difference between capacity and energy retentions are minor for all samples.

Figure 7 shows the voltage profiles of the (a) fresh, (b) 3 months, and (c) 1 year old NMC811 and the respective graphite electrodes, both versus the Li-reference electrode, of the cells depicted in Figure 6. As already discussed above, the voltage profiles of the graphite anodes show no significant changes in their polarization in dependence of the cycle number and only become 'shorter' due to the loss of specific capacity. The voltage profile of the fresh NMC811 (Figure 6a) slightly shifts to lower specific capacities, yet the potential difference between the charge and the discharge curve, i.e., the polarization stays fairly constant. The share of the specific capacity delivered during the CV-phase is 11.8% in the 5th cycle and 11.4% in the 312th cycle, underlining once more the constant polarization during cycling of the NMC811 without air contact. In contrast, the voltage profiles of the NMC811 stored at ambient air significantly widen with increasing cycle number (Figures 6b and 6c). This effect is even more pronounced for the one stored for 1 year at air compared to the one which was stored for 3 months. For the 3-months old NMC811 the specific capacity share of the CV-phase is significantly increased from 13.9% (5th cycle) to 23.0% (312th cycle), while it is increased even more from 14.2% (5th cycle) to 47.2% (312th cycle) for the 1 year old NMC811.

Discussion

Estimation of the surface layer thickness.—Our Raman and XPS data indicate that the formed carbonates are $NiCO_3$ species mixed with minor fractions of hydroxide and water. We believe that the rather low fractions of hydroxide and water are a consequence of the storage conditions as we stored the material at ambient air rather than at high temperature and/or high humidity. The latter conditions seem to favor hydroxide formation, as storage experiments with NMC622 at 55°C and 80% relative humidity conducted by Chen et al.[16] showed LiOH Raman bands, contrary to our observations (Figure 3). Additionally, these authors reported a weight increase of NMC622 at their conditions after six weeks of about 5%, roughly an order of magnitude higher than what we observed. The formation of $NiCO_3$ species is in contrast to the literature, in which the carbonate species are typically assigned to Li_2CO_3,[12,13,15–19,22] yet no clear evidence was provided for this assumption. Interestingly, Shizuka et al.[18] and Liu et al.[22] reported for both NCA and $LiNiO_2$ a partial reduction of Ni^{3+} to Ni^{2+} upon storage, yet they still assumed the carbonate species to be Li_2CO_3. However, if Li^+ is removed from the layered oxide structure, an oxidation of the Ni-ions would be expected. Therefore, we believe that the reported partial reduction of Ni^{3+} to Ni^{2+} is actually due to Ni-reduction upon formation of the $NiCO_3$ species.

The observed initial potential peak during the first charge (Figure 1) indicates that the surface impurity forms a resistive film around the NMC811 particles, which, at least partially, has to be decomposed before delithiation can occur, because the initial delithiation potential of the NMC actually lies at lower potentials than the initial voltage peak and should therefore happen before if there were no kinetic barriers. A similar initial potential peak was reported in the literature upon storage of NMC532[21] and $LiNiO_2$.[22] The (partial) decomposition of the surface impurity film is supported by the absence of the initial potential peak feature in the second and third charge cycle (Figure 1). In the following, we will estimate the surface layer thickness based on the determined carbonate contents summarized in Table I. In the patent by Paulsen et al., the equilibrium soluble base content (SBC), which is required to allow for a stable cycling performance, was measured using pH-titration and was determined to be ~20 $\mu mol/g_{NMC}$ for NMC622 with a BET surface area of 0.2 m^2/g.[15] If we assume that all the impurity is CO_3^{2-}, it corresponds to a weight fraction of 0.12 $\%_{wt}$, which is very close to the values shown in Table I for the fresh NMC811 and NMC111 electrodes. Therefore, the low carbonate contents of the fresh materials are most probably the carbonate from the equilibrium coverage, and the presence of any residual Li_2CO_3 from the synthesis can likely be excluded. In the following, we will estimate the total surface layer thickness, including the contribution from the equilibrium coverage layer.

The total surface layer thickness is estimated as a homogeneous, compact layer of $NiCO_3$ around the NMC particles. The particle radius r_{NMC} of the NMC particle was calculated using the BET-surface area and assuming spherical particles (Eq. 2) with a crystallographic density of NMC of $\rho_{NMC} = 4.8\ g/cm^3$.

$$r_{NMC} = \frac{3}{A_{BET} * \rho_{NMC}} \quad [2]$$

The volume V_{NMC} and mass m_{NMC} of a NMC particle can be calculated with the radius r_{NMC} and ρ_{NMC} (Eqs. 3 and 4).

$$V_{NMC} = \frac{4}{3 * \pi * r_{NMC}^3} \quad [3]$$

$$m_{NMC} = V_{NMC} * \rho_{NMC} \quad [4]$$

With the mass ratio of carbonate (Table I) multiplied by $M(NiCO_3)/M(CO_3^{2-}) = 1.98$ ($M(NiCO_3)$ is the molar mass of nickel

Downloaded on 2020-01-20 to IP 129.187.254.46 address. Redistribution subject to ECS terms of use (see ecsdl.org/site/terms_use) unless CC License in place (see abstract).

carbonate) and m_{NMC}, the mass of the surface layer m_L is calculated. Dividing m_L by the density $\rho_L = 4.358$ g/cm^3 [33] of $NiCO_3$ the volume of the surface layer V_L is obtained. Since the NMC particle including the surface impurity has the volume of $V_{NMC+L} = V_{NMC} + V_L$, the radius r_{NMC+L} can be calculated. By subtracting r_{NMC} from r_{NMC+L}, the layer thickness is obtained, as summarized in Table I. For NMC811, the total surface (carbonate) layer thickness after storage at ambient air increases from ∼2 nm (fresh NMC811) to ∼7 nm and ∼10 nm after three months and one year, respectively. This calculated layer thickness is in good agreement with the surface layer reported by Shkrob et al. using STEM.[21] For the obtained total surface layer thickness of ∼10 nm after one year of ambient air storage of the NMC811 sample, the O 1s oxygen lattice signal would be expected to be attenuated by 97% based on the estimated mean free path of ∼3 nm (as derived above), while the total surface layer thickness of the fresh sample (∼2 nm) would result in an attenuation by only ∼48%. This is consistent with the pronounced O 1s lattice signal for the fresh NMC811 sample and its complete absence for the 1-year old sample (Figure 4).

Consequences of the surface layer formation on NMC811 cells.—Our results clearly show that NMC811 is very sensitive to air contact, contrary to NMC111 for which no changes after one year of storage were observed. This illustrates a growing sensitivity to air with increasing nickel contents (possibly related to the growing Ni^{3+} content in Ni-rich NMCs) and makes it very crucial to store the material under inert atmosphere and to potentially use a controlled atmosphere during electrode processing like slurry preparation to maximize capacity and cycle-life. In Figure 6 we showed that the formation of surface impurities upon ambient storage has a very detrimental long-term effect on NMC811-graphite cells, as it causes the impedance on the NMC811 cathode to increase gradually (Figure 6b), leading to the observed decrease in cycling stability. This gradual impedance increase during cycling is larger as the exposure time to ambient air is increased and is not observed for the fresh NMC811 (Figure 6b). The presence of the initial potential peak only in the very first cycle (Figure 1) strongly suggests a decomposition of the carbonate surface layer during the first charge (to 4.4 V vs. Li/Li^+, Figure 1), which subsequently may cause the continuous impedance buildup. It may be possible that the products of the decomposed carbonate layer either decrease the electrochemical stability of the electrolyte or chemically react with the electrolyte forming a growing layer on the NMC particles, both of which may be observed as an increasing impedance on the NMC811 cathode. Additionally to the carbonate decomposition, a further cause of the steadily growing impedance may be due to a Li^+/H^+ exchange mechanism as proposed by Shkrob et al.[21] This mechanism may explain the increase of the specific capacity over the first ∼25 cycles of the 1-year old NMC811 cells in Figure 6 by removing the H^+ ions over several cycles and intercalating Li^+ ions from the electrolyte instead.[21] The presence of protons in the electrolyte may subsequently form HF with the $LiPF_6$ salt causing an etching of the NMC active material, which in consequence may cause the observed steady impedance increase. Nevertheless, to fully understand the exact underlying mechanism further studies are required. While it is beyond the scope of this work to explain the detailed mechanism underlying this observation, we believe that the involvement of nickel in the surface impurity is likely to be the reason for the irreversible damage to the NMC811 material, namely by inducing a surface reconstruction causing loss of active material and yielding a surface layer, which is most probably detrimental for the Li-diffusion. The latter is most likely the major reason for the very negative impact of the surface impurity, since the carbonate mass fractions in Table I are rather small, so that the overall active material loss by itself cannot explain the observed continuous long-term degradation of the NMC811-graphite cells (Figure 6). With this work we want to stress that the surface contamination has a detrimental long-term effect on NMC-graphite cells and therefore contact of Ni-rich materials to ambient air has to be avoided or at least reduced to a minimum in order to allow for stable cycling performance. Our results demonstrate that storage and handling of Ni-rich materials is a parameter of growing importance, when NMC111 is replaced by Ni-rich cathodes in Li-ion batteries.

Conclusions

In this work we reported on the severe surface reactivity of NMC811 compared to NMC111. We showed that even after one year of storage at ambient air, the NMC111 surface remained unchanged. In contrast, the amount of surface impurities increased significantly for the NMC811 samples stored for three months and one year under ambient conditions. In particular, we show that both NMC111 and NMC811 have initial carbonate contents of 0.07 – 0.08%$_{wt}$, which stay constant for NMC111 and increase by a factor of 5 to 0.39%$_{wt}$ for NMC811 after one year of ambient storage. Using Raman spectroscopy and XPS we found that the majority of the impurities formed on the NMC811 surface are carbonates with minor fractions of hydroxides and water. We clearly show that Ni is part of the surface impurity, which necessarily leads to extraction of Ni from the layered NMC structure, decomposing the surface of the NMC.

By cycling these NMC811 electrodes in NMC-graphite cells with a lithium reference electrode, we showed that ambient air storage of NMC811 not only leads to faster capacity fading rates, but also increases the impedance of the NMC811 cathode. On the other hand, the impedance of the graphite anode is not affected by the deterioration of the cathode, indicating the absence of obvious cross-talk effects as, for example, transition metal deposition on the anode. Therefore, our results clearly demonstrate that NMC811 should be stored under inert conditions and that its handling is due to the higher surface reactivity more challenging than NMC111, which has to be accounted for when NMC111 is replaced by NMC811 in Li-ion batteries.

Acknowledgment

The authors thank BMW AG for the financial support of this work. Umicore is greatly acknowledged for supplying the NMC materials. R.J. thanks TUM-IAS for their support in the frame of the Rudolf-Diesel Fellowship of Dr. Peter Lamp. This work made use of the MRSEC Shared Experimental Facilities at MIT, supported by the National Science Foundation under award number DMR-1419807.

References

1. D. Andre, S.-J. Kim, P. Lamp, S. F. Lux, F. Maglia, O. Paschos, and B. Stiaszny, *J. Mater. Chem. A*, **3**, 6709 (2015).
2. O. Groeger, H. A. Gasteiger, and J.-P. Suchsland, *J. Electrochem. Soc.*, **162**, A2605 (2015).
3. K. G. Gallagher, S. Goebel, T. Greszler, M. Mathias, W. Oelerich, D. Eroglu, and V. Srinivasan, *Energy Environ. Sci.*, **7**, 1555 (2014).
4. I. Belharouak, Y. K. Sun, J. Liu, and K. Amine, *J. Power Sources*, **123**, 247 (2003).
5. H.-J. Noh, S. Youn, C. S. Yoon, and Y.-K. Sun, *J. Power Sources*, **233**, 121 (2013).
6. I. Buchberger, S. Seidlmayer, A. Pokharel, M. Piana, J. Hattendorff, P. Kudejova, R. Gilles, and H. A. Gasteiger, *J. Electrochem. Soc.*, **162**, A2737 (2015).
7. R. Jung, M. Metzger, F. Maglia, C. Stinner, and H. A. Gasteiger, *J. Electrochem. Soc.*, **164**, A1361 (2017).
8. J. Li, L. E. Downie, L. Ma, W. Qiu, and J. R. Dahn, *J. Electrochem. Soc.*, **162**, A1401 (2015).
9. W. Liu, P. Oh, X. Liu, M.-J. Lee, W. Cho, S. Chae, Y. Kim, and J. Cho, *Angew. Chem., Int. Ed.*, **54**, 4440 (2015).
10. J. Zheng, W. H. Kan, and A. Manthiram, *ACS Appl. Mater. Interfaces*, **7**, 6926 (2015).
11. M. Gauthier, T. J. Carney, A. Grimaud, L. Giordano, N. Pour, H.-H. Chang, D. P. Fenning, S. F. Lux, O. Paschos, C. Bauer, F. Maglia, S. Lupart, P. Lamp, and Y. Shao-Horn, *J. Phys. Chem. Lett.*, **6**, 4653 (2015).
12. D. Aurbach, *J. Power Sources*, **89**, 206 (2000).
13. D. Aurbach, K. Gamolsky, B. Markovsky, G. Salitra, Y. Gofer, U. Heider, R. Oesten, and M. Schmidt, *J. Electrochem. Soc.*, **147**, 1322 (2000).
14. L. Giordano, P. Karayaylali, Y. Yu, Y. Katayama, F. Maglia, S. Lux, and Y. Shao-Horn, *J. Phys. Chem. Lett.*, **8**, 3881 (2017).
15. J. Paulsen and J. H. Kim, ed. US2014/0054495A1, USA, 2012.
16. Z. Chen, J. Wang, J. Huang, T. Fu, G. Sun, S. Lai, R. Zhou, K. Li, and J. Zhao, *Journal of Power Sources*, **363**, 168 (2017).
17. K. Matsumoto, R. Kuzuo, K. Takeya, and A. Yamanaka, *J. Power Sources*, **81–82**, 558 (1999).
18. K. Shizuka, C. Kiyohara, K. Shima, and Y. Takeda, *J. Power Sources*, **166**, 233 (2007).
19. J. M. Paulsen, H.-K. Park, and Y. H. Kwon, ed. US8574541, USA, 2013.

Downloaded on 2020-01-20 to IP 129.187.254.46 address. Redistribution subject to ECS terms of use (see ecsdl.org/site/terms_use) unless CC License in place (see abstract).

20. N. V. Faenza, L. Bruce, Z. W. Lebens-Higgins, I. Plitz, N. Pereira, L. F. J. Piper, and G. G. Amatucci, *J. Electrochem. Soc.*, **164**, A3727 (2017).
21. I. A. Shkrob, J. A. Gilbert, P. J. Phillips, R. Klie, R. T. Haasch, J. Bareño, and D. P. Abraham, *Journal of The Electrochemical Society*, **164**, A1489 (2017).
22. H. S. Liu, Z. R. Zhang, Z. L. Gong, and Y. Yang, *Electrochem. Solid-State Lett.*, **7**, A190 (2004).
23. M. Kerlau, M. Marcinek, V. Srinivasan, and R. M. Kostecki, *Electrochimica Acta*, **52**, 5422 (2007).
24. K. U. Schwenke, M. Metzger, T. Restle, M. Piana, and H. A. Gasteiger, *Journal of The Electrochemical Society*, **162**, A573 (2015).
25. A. T. Appapillai, A. N. Mansour, J. Cho, and Y. Shao-Horn, *Chemistry of Materials*, **19**, 5748 (2007).
26. Y.-C. Lu, A. N. Mansour, N. Yabuuchi, and Y. Shao-Horn, *Chemistry of Materials*, **21**, 4408 (2009).
27. M. P. Seah and W. A. Dench, *Surface and Interface Analysis*, **1**, 2 (1979).
28. J.-C. Dupin, D. Gonbeau, P. Vinatier, and A. Levasseur, *Physical Chemistry Chemical Physics*, **2**, 1319 (2000).
29. C. D. Wagner, D. A. Zatko, and R. H. Raymond, *Anal. Chem.*, **52**, 1445 (1980).
30. L. Salvati Jr., L. E. Makovsky, J. M. Stencel, F. R. Brown, and D. M. Hercules, *J. Phys. Chem.*, **85**, 3700 (1981).
31. R. B. Shalvoy, P. J. Reucroft, and B. H. Davis, *Journal of Catalysis*, **56**, 336 (1979).
32. G. Cherkashinin, D. Ensling, and W. Jaegermann, *J. Mater. Chem. A*, **2**, 3571 (2014).
33. F. Pertlik, *Acta Crystallogr., Sect. C: Cryst. Struct. Commun.*, **C42**, 4 (1986).
34. R. Dedryvere, D. Foix, S. Franger, S. Patoux, L. Daniel, and D. Gonbeau, *J. Phys. Chem. C*, **114**, 10999 (2010).
35. M. Metzger, B. Strehle, S. Solchenbach, and H. A. Gasteiger, *J. Electrochem. Soc.*, **163**, A798 (2016).
36. J. C. Burns, A. Kassam, N. N. Sinha, L. E. Downie, L. Solnickova, B. M. Way, and J. R. Dahn, *J. Electrochem. Soc.*, **160**, A1451 (2013).

Downloaded on 2020-01-20 to IP **129.187.254.46** address. Redistribution subject to ECS terms of use (see **ecsdl.org/site/terms_use**) unless CC License in place (see abstract).